BBA - Molecular Basis of Disease 1865 (2019) 391–402

Contents lists available at ScienceDirect

BBA - Molecular Basis of Disease

journal homepage: www.elsevier.com/locate/bbadis

# CXCR6 protects from inflammation and fibrosis in NEMO$^{LPC-KO}$ mice

Anke Liepelt[a,1], Alexander Wehr[a,1], Marlene Kohlhepp[a], Jana C. Mossanen[a,b], Karina Kreggenwinkel[a], Bernd Denecke[c], Ivan G. Costa[d], Tom Luedde[a], Christian Trautwein[a], Frank Tacke[a,*]

[a] Department of Medicine III, RWTH-University Hospital Aachen, Pauwelsstr. 30, 52074 Aachen, Germany
[b] Department of Intensive and Intermediate Care, RWTH-University Hospital Aachen, Pauwelsstr. 30, 52074 Aachen, Germany
[c] Chip Facility, IZKF Aachen, University Hospital, RWTH Aachen University, Pauwelsstr. 30, 52074 Aachen, Germany
[d] IZKF Computational Biology Research Group, University Hospital, Pauwelsstraße 19, RWTH Aachen University, 52074 Aachen, Germany

ARTICLE INFO

*Keywords:*
Liver fibrosis
Inflammation
Hepatocytes
Chemokine receptor

ABSTRACT

Chronic inflammation in the liver provokes fibrosis and, on long-term, carcinogenesis. This sequence is prototypically recapitulated in mice with hepatocyte-specific knock-out of the NF-κB essential modulator (NEMO), termed NEMO$^{LPC-KO}$ mice, in which increased hepatocyte apoptosis and compensatory regeneration cause steatosis, inflammation and fibrosis. Natural killer T (NKT) cells carrying the chemokine receptor CXCR6 participate in liver inflammation and injury responses. Here, we investigated the role of CXCR6 in the NEMO$^{LPC-KO}$ mouse model. Unexpectedly, genetic deletion of CXCR6 enhanced hepatocyte death, inflammation and fibrosis in NEMO$^{LPC-KO}$ mice. Although CXCR6 expression is restricted to immune cells in the liver, the adoptive transfer of CXCR6$^+$ cells did not protect NEMO$^{LPC-KO}$*Cxcr6*$^{-/-}$ mice from hepatic injury. Gene array analyses revealed up-regulated stress response and metabolism pathways in hepatocytes from NEMO$^{LPC-KO}$*Cxcr6*$^{-/-}$ mice, functionally corresponding to an increased susceptibility of these hepatocytes to TNFα-induced cell death in vitro. These data revealed a novel CXCR6-dependent mechanism of suppressing inflammatory hepatocytic responses to cellular stress.

## 1. Introduction

Deletion of the nuclear factor kappa-B (NF-κB) essential modulator (NEMO) also known as NF-κB inhibitor of kinase subunit gamma (IKK-γ) in liver parenchymal cells (LPC) causes spontaneous development of increased hepatocyte apoptosis and compensatory regeneration leading to a sequence of steatohepatitis, fibrosis and, ultimately, liver cancer [1], making this a well-suited mouse model to study mechanisms of inflammation-driven hepatocarcinogenesis [2]. In hepatocytes, NF-κB is activated in response to stress signals like TNF-α via transforming growth factor beta-activated kinase 1 (TAK1) and NEMO, preventing cleavage and activation of caspase 8 [3]. In contrast, in hepatocytes where NEMO is absent, NF-κB signaling is blocked leading to cleavage of caspase 8 and 3 and subsequently to hepatocyte apoptosis [1,3]. Hepatocyte death then triggers a chronic inflammatory and a regenerative response in the liver finally leading to the development of hepatocellular carcinoma [4]. While these hepatocyte-intrinsic pathways have been widely explored in the model of hepatocyte-specific NEMO knock-out (NEMO$^{LPC-KO}$) mice, the immune responses driving inflammation and fibrosis are less well understood.

In the liver, the chemokine receptor CXCR6 is predominantly expressed on lymphocytes (NKT, NK, CD4$^+$ and CD8$^+$ T cells), but not on macrophages or neutrophils [5,6]. Its only known ligand CXCL16 is a transmembrane chemokine expressed by liver sinusoidal endothelial cells [6]. The lymphocyte migration, especially of NKT cells, directed by CXCR6 and CXCL16 amplifies the hepatic inflammation early in the course after injury, thereby stimulating long-term consequences of liver injury like fibrosis [7]. Intravital imaging studies demonstrated that CXCR6$^+$ NKT cells patrol hepatic sinusoids and accumulate upon acute and chronic liver injury, thereby promoting an inflammatory response [5,6,8]. When CXCR6 is absent, mice are protected from fibrosis progression in two experimental models of liver fibrosis [5]. In particular, feeding mice with a methionine and choline-deficient (MCD) diet or repetitively administering the hepatotoxin carbon tetrachloride ($CCl_4$) demonstrated that CXCR6 is required for early NKT cell accumulation in the injured livers, thereby supporting a cascade of cellular and

* Corresponding author at: Department of Medicine III, University Hospital Aachen, Pauwelsstrasse 30, 52074 Aachen, Germany.
*E-mail address:* frank.tacke@gmx.net (F. Tacke).
[1] These authors contributed equally to this work.

https://doi.org/10.1016/j.bbadis.2018.11.020
Received 3 July 2018; Received in revised form 16 October 2018; Accepted 22 November 2018
Available online 24 November 2018
0925-4439/ 

**Abbreviations**

| | |
|---|---|
| ALT | alanine aminotransferase |
| AST | aspartate aminotransferase |
| FDR | false discovery rate |
| GLDH | glutamate dehydrogenase |
| GOEA | Gene Ontology Enrichment Analysis |
| LDH | lactate dehydrogenase |
| LPC | liver parenchymal cells |
| NEMO | NF-κB essential modulator |
| NF-κB | nuclear factor kappa-B |
| SOM | self-organizing maps |
| wt | wildtype |

molecular events characterized by inflammatory cytokine production, macrophage recruitment and fibrogenesis [5]. Recent reports further demonstrated the importance of the CXCR6/CXCL16 axis in non-alcoholic fatty liver disease (NAFLD). In casein-injected mice, a model for inflamed NAFLD, expression of both CXCR6 and CXCL16 are induced and involved in the progression of the disease [9]. Serum CXCL16 levels are significantly increased in patients with NAFLD and fibrosis [10,11]. Co-culture experiments with hepatocytes and hepatic stellate cells

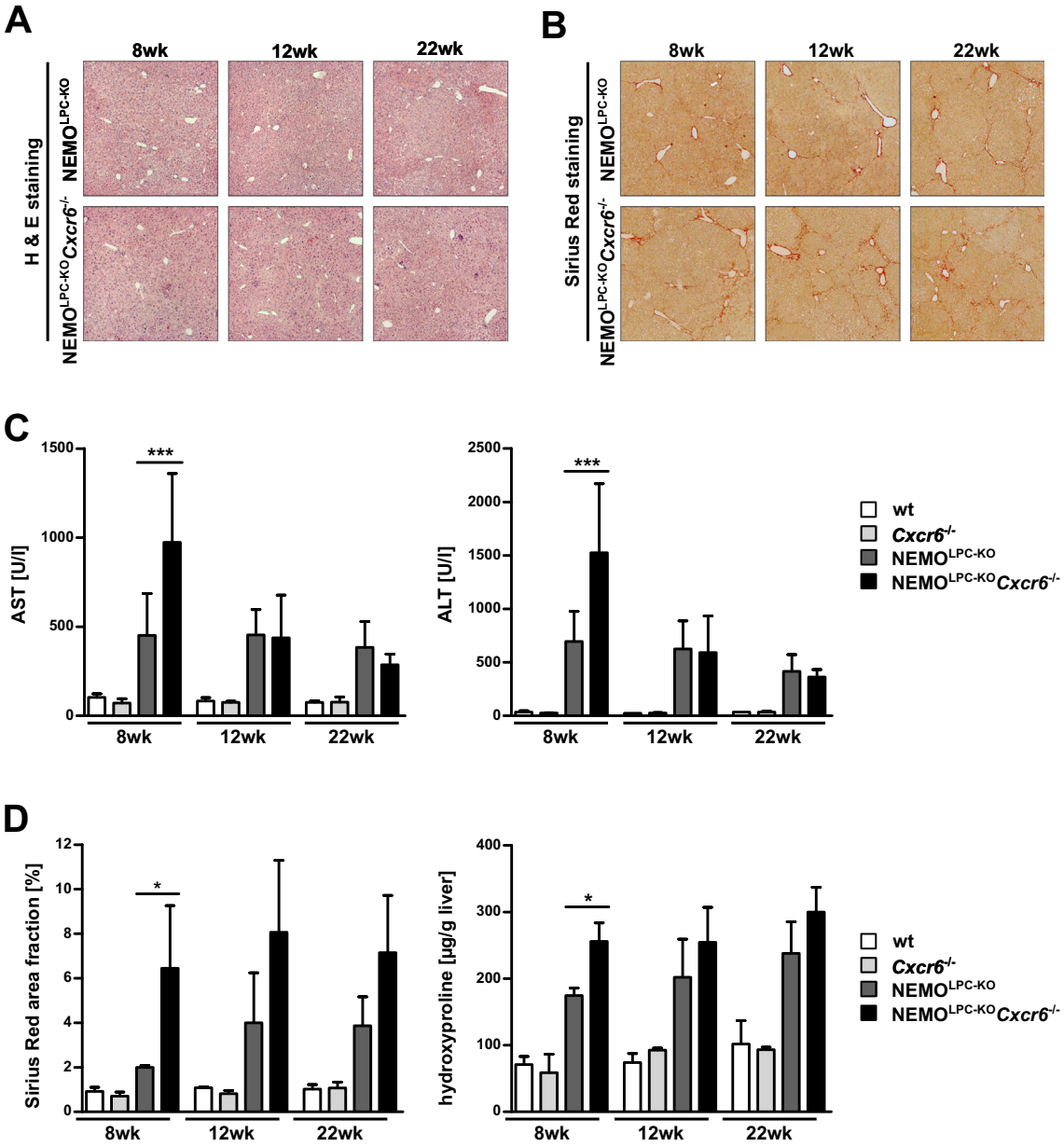


**Fig. 1.** NEMO$^{LPC\text{-}KO}$*Cxcr6*$^{-/-}$ mice display enhanced liver damage and fibrosis progression compared to NEMO$^{LPC\text{-}KO}$ mice. (A) H&E stainings of liver paraffin sections from 8, 12 and 22 week old NEMO$^{LPC\text{-}KO}$ and NEMO$^{LPC\text{-}KO}$*Cxcr6*$^{-/-}$ mice. (B) Collagen deposition in liver sections from 8, 12 and 22 week old NEMO$^{LPC\text{-}KO}$ and NEMO$^{LPC\text{-}KO}$*Cxcr6*$^{-/-}$ mice visualized by Sirius Red staining, representative images are shown. (C) Hepatic injury was assessed by quantification of serum aspartate transaminase (AST) and alanine transaminase (ALT) activities. Biological replicates of n = 3 to 23 animals per data point. (D) Quantification of Sirius Red staining shown in Fig. 1B (left panel) and intrahepatic hydroxyproline content (right panel) to assess hepatic collagen. Biological replicates of n = 3 to 11 animals per data point. All data are represented as mean ± SD. *p < 0.05, ***p < 0.001 (one-way ANOVA).

(HSCs) lead to the conclusion that CXCL16 contributes to steatotic and fibrotic progression and hence could serve as a biomarker as well a therapeutic target for NAFLD [11]. In line, blocking this pathway by an anti-CXCL16 antibody inhibited inflammatory macrophage infiltration and steatosis in the MCD model [12], providing a proof-of-concept for the therapeutic potential of targeting this chemokine receptor axis.

In this study, we set out experiments to clarify the role of CXCR6-dependent mechanisms on inflammation and fibrosis in the NEMO$^{LPC-KO}$ mouse model. Surprisingly, genetic deletion of *Cxcr6* aggravated inflammation and fibrosis in the NEMO$^{LPC-KO}$ mice, unravelling a novel role of CXCR6 for stress responses in hepatocytes, which is independent from the functions of CXCR6 on immune cells.

## 2. Materials and methods

### 2.1. Mice

Nemo-cre$^{-}$ (wildtype, wt), Nemo-cre$^{-}$/*Cxcr6*$^{eGfp/eGfp}$ (*Cxcr6*$^{-/-}$), Nemo-cre$^{+}$ (NEMO$^{LPC-KO}$) and Nemo-cre$^{+}$/*Cxcr6*$^{eGfp/eGfp}$ (NEMO$^{LPC-KO}$*Cxcr6*$^{-/-}$) mice were housed under specific pathogen free conditions. All experiments were performed with male mice, have been approved by the appropriate authorities according to German legal requirements and were carried out in accordance with the EU Directive 2010/63/EU for animal experiments. The transgenic Cxcr6 eGfp knock-in mice (*Cxcr6*$^{eGfp/eGfp}$) lack functional CXCR6 [13]. The NEMO$^{LPC-KO}$ mice carry loxP-site-flanked (floxed) alleles of the Nemo gene (NemoFl) and were crossed to Alfp-Cre transgenic mice to generate a liver parenchymal cell-specific knockout of Nemo [1]. To generate NEMO$^{LPC-KO}$*Cxcr6*$^{eGfp/eGfp}$ mice, NEMO$^{LPC-KO}$ mice were crossed with *Cxcr6*$^{eGfp/eGfp}$ mice. Genotypes were confirmed via PCR specific for the respective alleles using DNA from tail or ear biopsies.

### 2.2. Liver enzymes, hydroxyproline quantification, histology and immunohistochemistry

Aspartate aminotransferase (AST), alanine aminotransferase (ALT), lactate dehydrogenase (LDH) and glutamate dehydrogenase (GLDH) activities were measured (UV test at 37 °C) in serum or supernatant (Roche Modular pre-analytics system, Rotkreuz, Switzerland). The hepatic hydroxyproline content (reflecting total intrahepatic collagen) was measured as described before [14]. Conventional hematoxylin-eosin (H&E) and Sirius Red staining was performed according to established protocols [12]. Liver sections from fixed paraffin blocks were immunohistochemically stained according to standard procedures using anti-mouse F4/80 and anti-mouse phosho-c-Jun (Cell signaling) antibodies. Stainings were evaluated by quantifying the area fraction or number of positively stained hepatocytes using ImageJ Software (NIH) [15].

### 2.3. Analysis of intrahepatic leukocytes

Livers were digested by collagenase type IV (Worthington, USA), and intrahepatic leukocytes were isolated by multiple differential centrifugation steps as described earlier [16]. All cells were subjected to red cell lysis by Pharmlyse (BD Biosciences) and stained with fluorochrome-conjugated antibodies for multi-color fluorescent-activated cell sorting (FACS) analysis. Analysis was performed using LSR-Fortessa (BD Biosciences), and cell sorting was done by using the FACS Aria-II-SORP (BD Biosciences). Data analysis was done by using FlowLogic (Inivai, Victoria, Australia) and FlowJo (Ashland, USA).

### 2.4. Quantitative PCR

Liver tissue was shock-frozen in liquid nitrogen and stored at −80 °C. RNA was purified by pegGOLD (peqLab, Erlangen, Germany) using standard protocols. Complementary DNA was generated from 1 μg RNA using a complementary DNA synthesis kit (Roche, Basel, Switzerland). Quantitative real-time PCR was performed using SYBR green reagent (Invitrogen, Darmstadt, Germany). β-actin was used to normalize the gene expression. Primer sequences are available upon request.

### 2.5. Immunoblot analysis

Protein lysates were prepared from primary hepatocytes or liver samples, separated by SDS-polyacrylamide gel electrophoresis (PAGE), transferred to nitrocellulose, and analyzed by immunoblotting. Membranes were probed with the following antibodies: anti-ERK, anti-phospho-ERK, anti-JNK, anti-phospho-JNK, anti-cleaved caspase 3 (Cell Signaling); anti-PCNA (Zymed); anti-GAPDH (Abd Serotec); anti-α-SMA (Sigma Aldrich). As secondary antibodies, anti-rabbit-HRP, anti-mouse-HRP, and anti-rat-HRP were used (GE Healthcare).

### 2.6. Adoptive cell transfer

CXCR6-expressing leukocytes were FACS-sorted from livers of healthy heterozygous *Cxcr6*$^{eGfp/+}$ mice. $1 \times 10^6$ cells were adoptively transferred into NEMO$^{LPC-KO}$ or NEMO$^{LPC-KO}$*Cxcr6*$^{-/-}$ mice once per week between weeks 4 and 8 of age via i.v. injection into the lateral tail vein.

### 2.7. Isolation, culture and treatment of primary hepatocytes

Primary hepatocytes from 12 weeks old mice were isolated and cultured, as previously described [15]. Cells were treated with 100 ng TNF-α or PBS as control for 10 h and cell culture supernatant was harvested for enzyme analysis. 12 week old mice were chosen, because basal levels of hepatocyte damage were comparable at this time point (see Fig. 1C).

### 2.8. Microarray gene expression analysis

Gene expression in freshly isolated primary hepatocytes from 12 week old mice (biological replicates) was analyzed using the GeneChip® MTA 1.0 st (Affymetrix, Santa Clara, CA, USA). Total RNA was isolated using Qiagen RNAeasy kit and quantified (Nanodrop 8000 (Thermo Scientific, Waltham, MA, USA)). RNA quality was assessed using RNA 6000 Nano Assay with the 2100 Bioanalyzer (Agilent, Santa Clara, CA, USA) to ensure that the samples had a RNA integrity number (RIN) of at least 7.3. Samples were prepared and hybridized to the GeneChip® MTA 1.0 st Arrays according to the GeneChip® WT Plus Reagent Kit user manual (P/N 703174 Rev. 2; Affymetrix). Briefly, for each sample, 300 ng of total RNA was reverse-transcribed into cDNA using a random hexamer oligonucleotide tagged with a T7 promoter sequence. After second strand synthesis, double-stranded cDNA was used as a template for amplification with T7 RNA polymerase to obtain antisense cRNA. Random hexamers and dNTPs spiked with dUTPs were used to reverse-transcribe the cRNA into single-stranded sense strand cDNA. The cDNA was fragmented by uracil DNA glycosylase and apurinic/apyrimidic endonuclease 1. Fragment size was checked using the 2100 Bioanalyzer (fragment size between 50 and 200 bp). Fragmented sense cDNA was biotin-endlabelled with Terminal Deoxynucleotidyl Transferase (TdT) and hybridized to GeneChip® MTA 1.0 st Arrays at 45 °C for 16 h with 60 rpms. Hybridized arrays were washed and stained on a Fluidics Station 450 (program: FS450 0001) and scanned on a GeneChip® Scanner 3000 7G (both Affymetrix). Raw image data was analyzed with Affymetrix® Expression Console™ Software, and gene expression intensities were normalized and summarized with robust multiarray average (RMA) algorithm [17]. Statistical tests for differential expression were performed using Affymetrix® Transcriptome Analysis Console (TAC) Software, which computes and summarizes a traditional unpaired One-Way (single factor) Analysis of

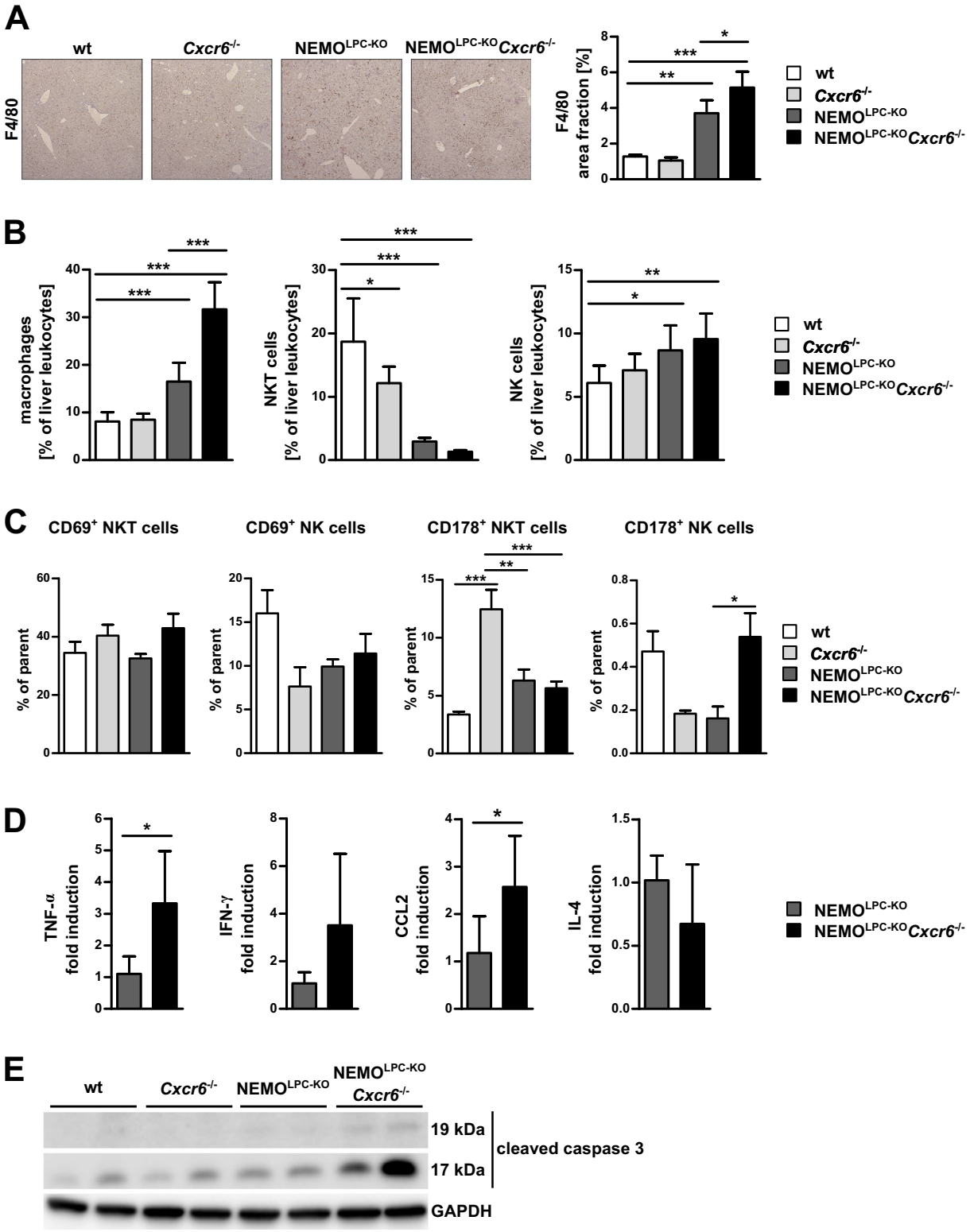


**Fig. 2.** NEMO$^{LPC\text{-}KO}$*Cxcr6*$^{-/-}$ mice are hallmarked by a pro-inflammatory, pro-apoptotic liver environment. (A) Immunohistochemical staining for the macrophage marker F4/80 in liver sections of 8 week old mice. Representative images (left panel), quantification of F4/80 area fraction (right panel). Biological replicates of n = 3 to 8 animals per genotype. (B) FACS analysis of liver leukocyte populations of 8 week old mice. Biological replicates of n = 6 to 10 animals per genotype. (C) Characterization of hepatic NKT and NK cells of 12 week old mice by FACS analysis. Biological replicates of n = 3 to 9 animals per genotype. (D) Relative mRNA expression of TNF-α, IFN-γ, CCL2 and IL-4 in whole liver tissue of 8 week old NEMO$^{LPC\text{-}KO}$ and NEMO$^{LPC\text{-}KO}$*Cxcr6*$^{-/-}$ mice normalized to β-actin mRNA. Biological replicates of n = 5 to 7 animals per genotype. (E) Activation of caspase 3 by cleavage to 17 and 19 kDa fragments was analyzed by immunoblotting in lysates from isolated hepatocytes from 8 week old mice. Biological replicates of n = 2 animals per genotype. All data are represented as mean ± SD. *$p < 0.05$, **$p < 0.01$, ***$p < 0.001$ (one-way ANOVA for (A), (B) and (C) or unpaired student's *t*-test for (D)).

Variance (ANOVA) for each condition group. Microarray raw data is deposited in Gene Expression Omnibus (GEO) under the accession number GSE121124.

### 2.9. Statistical and bioinformatics analysis

All data are presented as mean ± standard deviation (SD). Differences between groups were assessed by using the appropriate statistical tests (GraphPad prism 5, La Jolla, USA). For SOM, pre-processed microarray intensity data in log-scale was used as input for the analysis with the R-package oposSOM [18]. The size of the square SOM grid was set to 30 × 30 with all other parameters at default settings. For selection of genotype-specific metagenes, k-means hierarchical clustering was chosen [19]. Genes from selected clusters were subjected to gene ontology enrichment analysis (GOEA) using the PANTHER [20] statistical overrepresentation test with default settings and a reference set containing all transcripts from the MTA 1.0 st Arrays. For enrichment maps, differentially expressed genes were selected by a raw ANOVA p-value threshold of ≤0.05 and a fold change of at least 2 or −2 respectively. Selected differentially expressed genes were subjected to GOEA (GO biological process) by using the Cytoscape [21] plug-in BinGO [22]. For network visualization, the Cytoscape plugin Enrichment Map [23] was used. For enrichment map visualization, the following criteria were chosen: p-value ≤ 0.01, FDR Q-value cutoff ≤0.1, similarity cutoff with Jaccard coefficient ≤0.3.

## 3. Results

### 3.1. $NEMO^{LPC\text{-}KO}Cxcr6^{-/-}$ mice display enhanced liver damage and fibrosis compared to $NEMO^{LPC\text{-}KO}$ mice

We investigated the influence of *Cxcr6* deletion on the extent of liver injury in mice with a knock-out of NEMO in liver parenchymal cells ($NEMO^{LPC\text{-}KO}$). $NEMO^{LPC\text{-}KO}$ mice displayed a disturbed liver histology with areas of apoptotic hepatocytes as early as at the age of 8 weeks (Fig. 1A). $NEMO^{LPC\text{-}KO}$ mice deficient for CXCR6 developed a more aggravated injury phenotype, especially at 8 weeks of age, with progressive lesions until the age of 22 weeks (Fig. 1A). No macroscopic tumor lesions ≥5 mm were visible in either genotype until 22 weeks of age (Suppl. Fig. 1A). $NEMO^{LPC\text{-}KO}$ mice were reported to spontaneously develop moderate hepatic fibrosis at 12 weeks of age [1]. In our experiments, Sirius Red staining for collagen deposition was already detectable at 8 weeks of age, and fibrosis progressed over the period of the experiment (Fig. 1B). Collagen deposition appeared enhanced in $NEMO^{LPC\text{-}KO}Cxcr6^{-/-}$ mice, especially at the early time-points investigated (Fig. 1B). In line with the histological assessments, the double knockout animals displayed increased liver damage in the early course of the experimental model compared to $NEMO^{LPC\text{-}KO}$ mice as measured by serum transaminase activities (Fig. 1C). Quantification of collagen deposition by Sirius Red staining, measurement of total intrahepatic hydroxyproline content and of the myofibroblast activation marker α-smooth muscle actin (α-SMA) confirmed enhanced fibrogenesis in $NEMO^{LPC\text{-}KO}Cxcr6^{-/-}$ mice (Fig. 1D and Suppl. Fig. 1B). Thus, unexpectedly, deletion of *Cxcr6* aggravates liver injury and fibrogenesis in $NEMO^{LPC\text{-}KO}$ mice.

### 3.2. $NEMO^{LPC\text{-}KO}Cxcr6^{-/-}$ mice are hallmarked by a pro-inflammatory and pro-apoptotic liver environment

Deletion of NEMO in LPC including hepatocytes and biliary epithelial cells, but not endothelial or Kupffer cells, induces a chronic inflammatory response in the liver [1]. In liver sections stained for the macrophage marker F4/80, macrophages significantly increased in 8 weeks old $NEMO^{LPC\text{-}KO}$ and $NEMO^{LPC\text{-}KO}Cxcr6^{-/-}$ in comparison to NEMO-proficient wildtype (wt) mice (Fig. 2A). In line with the observed enhanced liver damage in $NEMO^{LPC\text{-}KO}Cxcr6^{-/-}$ mice (Fig. 1C),

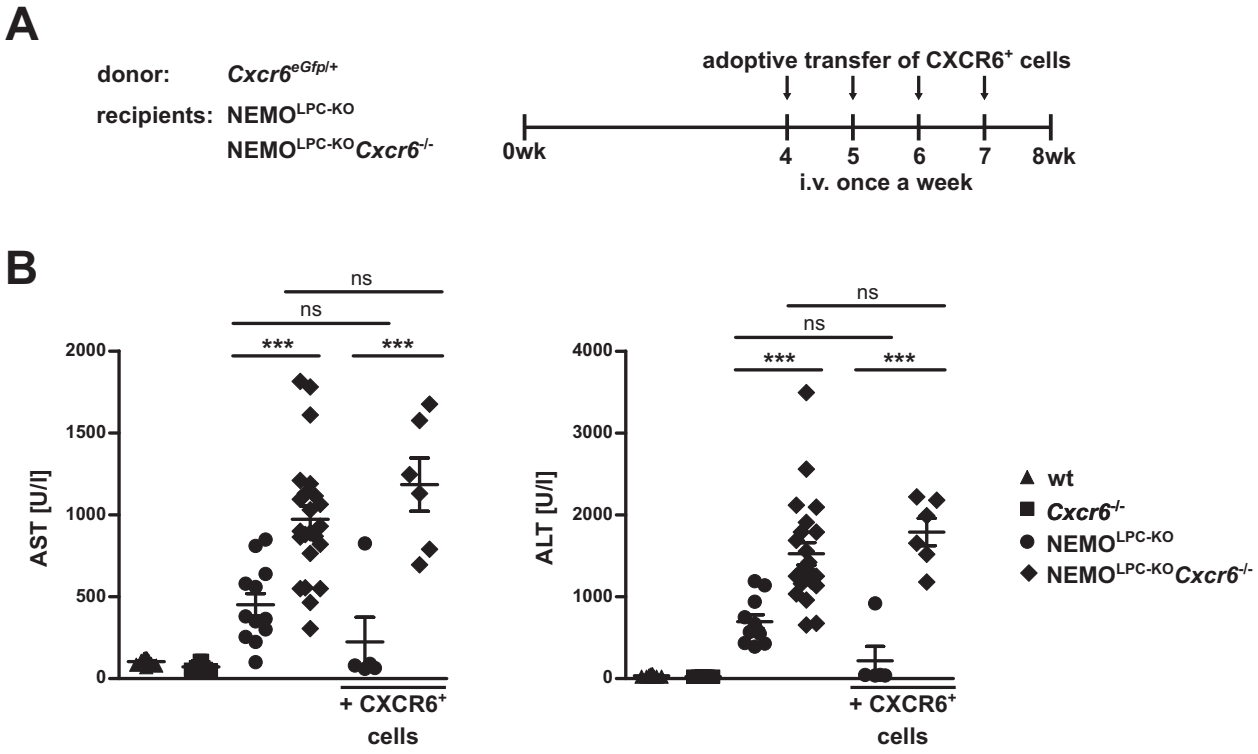


**Fig. 3.** Adoptive transfer of CXCR6$^+$ cells is not able to protect $NEMO^{LPC\text{-}KO}Cxcr6^{-/-}$ mice from hepatic injury. (A) CXCR6$^+$ cells isolated from livers of healthy heterozygous $Cxcr6^{eGfp/+}$ mice were adoptively transferred into $NEMO^{LPC\text{-}KO}$ or $NEMO^{LPC\text{-}KO}Cxcr6^{-/-}$ mice once per week starting at week 4. Animals were analyzed at 8 weeks of age. (B) Hepatic injury was assessed by quantification of serum aspartate transaminase (AST) and alanine transaminase (ALT) activities. Biological replicates of n = 5 to 23 animals per data point. All data are represented as mean ± SD. ***p < 0.001 (one-way ANOVA).

F4/80 staining was highest in the double knockout mice (Fig. 2A). To investigate the influence of different immune cell populations in more detail, liver leukocytes were analyzed by FACS from 8 week old mice. Macrophages were strongly augmented in NEMO$^{LPC-KO}$ and NEMO$^{LPC-KO}$*Cxcr6*$^{-/-}$ mice with a significantly higher cell number in NEMO$^{LPC-KO}$*Cxcr6*$^{-/-}$ mice (Fig. 2B), confirming the immunohistochemical results (Fig. 2A). CXCR6 is predominantly expressed on lymphocytes, especially on NKT cells, but not on macrophages or neutrophils [5]. In fact, > 80% of hepatic NKT cells, and 40–60% of NK and T cells in the liver carry CXCR6 (Suppl. Fig. 1C). Thus, deletion of *Cxcr6* depleted the number of hepatic NKT cells (Fig. 2B, compare wt with *Cxcr6*$^{-/-}$, or NEMO$^{LPC-KO}$ with NEMO$^{LPC-KO}$*Cxcr6*$^{-/-}$). As expected, the number of liver macrophages was unaffected by the *Cxcr6* knockout, but increased in injured livers of NEMO$^{LPC-KO}$ mice and was even higher in the double knockout (Fig. 2B). In addition, NK cells, which also express CXCR6, were moderately upregulated. Regarding lymphocyte activation markers, the proportion of CD69$^+$ NKT and NK cells was moderately, but not significantly affected by the genotype (Fig. 2C, left panels). CD69 is an early marker for lymphocyte activation. Binding of CD178 (Fas ligand) to its receptor Fas induces apoptosis and thus contributes to the regulation of immune responses. In *Cxcr6*$^{-/-}$ mice CD178 is significantly upregulated on NKT cells and downregulated on NK cells compared to wt. In NEMO$^{LPC-KO}$ mice a slight upregulation in NKT cells and a downregulation in NK cells was observed (Fig. 2C, right panels). However, NKT cells from double knockout mice were not significantly altered in their CD178 expression compared to both wt and NEMO$^{LPC-KO}$. In NEMO$^{LPC-KO}$*Cxcr6*$^{-/-}$ mice there were significantly more CD178$^+$ NK cells, but their overall percentage was quite low (< 1%). Gene expression levels of the pro-inflammatory cytokines TNF-α and IFN-γ as well as CCL2, a cytokine responsible for macrophage attraction, were strongly induced in NEMO$^{LPC-KO}$*Cxcr6*$^{-/-}$ mice compared to NEMO$^{LPC-KO}$ mice, while the anti-inflammatory IL-4 mRNA was reduced in NEMO$^{LPC-KO}$*Cxcr6*$^{-/-}$ mice (Fig. 2D). Moreover, cleavage of caspase 3 was augmented in NEMO$^{LPC-KO}$*Cxcr6*$^{-/-}$ mice (Fig. 2E). Cleavage and thereby activation of caspase 3 is an early event during programmed cell death in response to e.g. TNF-α. These data demonstrate the activation of inflammatory macrophages and the establishment of a pro-inflammatory immune response in livers of NEMO$^{LPC-KO}$*Cxcr6*$^{-/-}$ mice, alongside increased hepatocyte cell death and injury.

### 3.3. Adoptive transfer of CXCR6$^+$ cells is not able to protect NEMO$^{LPC-KO}$*Cxcr6*$^{-/-}$ mice from hepatic injury

Next, we investigated whether the lack of CXCR6-expressing immune cells was responsible for the aggravated phenotype in NEMO$^{LPC-KO}$*Cxcr6*$^{-/-}$ mice. We thus tested, if it is possible to rescue NEMO$^{LPC-KO}$*Cxcr6*$^{-/-}$ mice from the enhanced liver damage by adoptively transferring CXCR6-expressing cells from livers of CXCR6-reporter mice (*Cxcr6*$^{eGfp/+}$), which includes different CXCR6$^+$ immune cells (liver NKT, NK, T cells). The rationale for this experiment was based on the fact that CXCR6$^+$ immune cells were lacking in NEMO$^{LPC-KO}$*Cxcr6*$^{-/-}$ mice, which particularly resulted in lack of hepatic NKT cells in these animals. CXCR6$^+$ cells were transferred into NEMO$^{LPC-KO}$ or NEMO$^{LPC-KO}$*Cxcr6*$^{-/-}$ mice beginning at 4 weeks of age, once per week until week 8 (Fig. 3A). Strikingly, liver damage, as judged by serum transaminase activities, of NEMO$^{LPC-KO}$ mice was strongly reduced after transfer of CXCR6$^+$ cells. In contrast, the adoptive transfer did not alter the observed liver damage in NEMO$^{LPC-KO}$*Cxcr6*$^{-/-}$ mice (Fig. 3B). Collectively, the data demonstrated that CXCR6 expressing immune cells are unable to ameliorate the liver injury phenotype of NEMO$^{LPC-KO}$*Cxcr6*$^{-/-}$ mice, indicating that the NEMO-deficient hepatocytes in NEMO$^{LPC-KO}$*Cxcr6*$^{-/-}$ mice may be intrinsically more susceptible to injury signals.

### 3.4. Stress response and metabolism pathways are upregulated in hepatocytes from NEMO$^{LPC-KO}$*Cxcr6*$^{-/-}$ mice

We hypothesized that the hepatocytes themselves are primed towards injury due to the lack of signals from CXCR6$^+$ cells or CXCR6 signaling itself. We therefore comprehensively studied the transcriptomes of hepatocytes from the different mouse strains. Gene expression of isolated hepatocytes was analyzed by microarray, followed by a co-regulation gene analysis and visualization strategy based on self-organizing maps (SOM) machine learning [18]. This method employs a self-organizing map to cluster single gene expression values to metagenes. Based on these metagenes, visualizations (e.g. expression portraits) or downstream sample similarity analyses are performed. Expression portraits serve as fingerprints of the transcriptional activity of the respective samples. Visualization of metagene expression in expression portraits of the four sample groups showed that the transcriptional similarity was highest between wt and *Cxcr6*$^{-/-}$ hepatocytes and the two genotypes with NEMO$^{LPC-KO}$ background, respectively (Fig. 4A). A second unsupervised dimension reduction step led to the detection of over- or underexpression spots representing clusters of co-expressed metagenes, which are highly regulated in, at minimum, one sample. K-means clustering was applied revealing 15 clusters of co-expressed genes (Fig. 4B, left). The sample-to-cluster-correlation showed specific clusters of genes with low expression (cluster B) and high expression (clusters L and O), respectively, in only the NEMO$^{LPC-KO}$*Cxcr6*$^{-/-}$ hepatocytes (Fig. 4B, right). A list of the transcripts belonging to each cluster is provided in Suppl. Table S1. Plotting of the standardized mRNA expression in a heatmap reflected the correlation of the clusters and the expression of individual genes in the NEMO$^{LPC-KO}$*Cxcr6*$^{-/-}$ samples (Fig. 4C, Suppl. Fig. S2). To relate the individual clusters to a biological function, a statistical overrepresentation test (Gene Ontology Enrichment Analysis (GOEA)) using the PANTHER database with GO-slim Biological Process annotation data set was done for cluster L, which contains transcripts only upregulated in hepatocytes of NEMO$^{LPC-KO}$*Cxcr6*$^{-/-}$ mice. Besides phagocytosis, MAPK cascade was one of the most highly overrepresented biological process terms (Suppl. Table S2). Testing transcripts in cluster B and O did not yield any statistically significant results.

To understand the functional relevance of the differences in mRNA expression between NEMO$^{LPC-KO}$*Cxcr6*$^{-/-}$ and NEMO$^{LPC-KO}$ mice, we performed GOEA of significantly regulated genes. Differentially expressed genes were selected by their fold change of at least 2 or −2 and an ANOVA p-value ≤ 0.05. 125 genes were significantly upregulated and 36 genes were significantly downregulated comparing hepatocytes from NEMO$^{LPC-KO}$*Cxcr6*$^{-/-}$ vs. NEMO$^{LPC-KO}$ mice. These genes were then analyzed for overrepresentation of Gene Ontology biological process terms, and functional differences were visualized in an Enrichment Map network (Fig. 5A). This analysis showed that processes like activation of innate immune response or response to stress were upregulated in NEMO$^{LPC-KO}$*Cxcr6*$^{-/-}$ mice, which is in agreement with the experimental data. In addition, biological processes terms related to fatty acid and lipoprotein metabolism were also overrepresented in our analysis. GOEA analysis and Enrichment Map visualization of *Cxcr6*$^{-/-}$ vs. wt mice did not result in a differentiated functional network although a similar number of genes was regulated (Fig. 5B), confirming that not the *Cxcr6* deletion per se but their occurrence in a hepatocyte stress environment (NEMO$^{LPC}$) determined the susceptibility to liver injury.

To explore this regulation in more detail, differentially regulated genes were selected comparing NEMO$^{LPC-KO}$*Cxcr6*$^{-/-}$ vs. NEMO$^{LPC-KO}$ and *Cxcr6*$^{-/-}$ vs. wt by using the following criteria: p-value ≤ 0.01 and log2 fold change of ≥2 or ≤ −2 (Fig. 6A). The fold change regulation of NEMO$^{LPC-KO}$*Cxcr6*$^{-/-}$ vs. NEMO$^{LPC-KO}$ was plotted against the corresponding p-values in a volcano plot (Fig. 6B). Significantly regulated genes were highlighted by the blue boxes and the 26 transcripts only differentially regulated on the NEMO$^{LPC-KO}$ background were marked

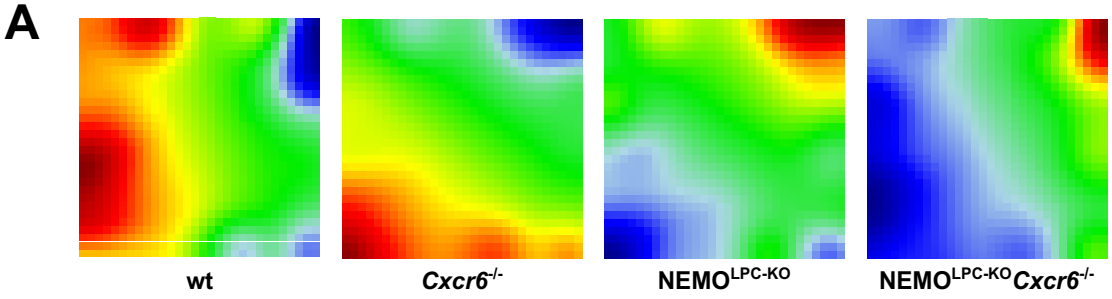


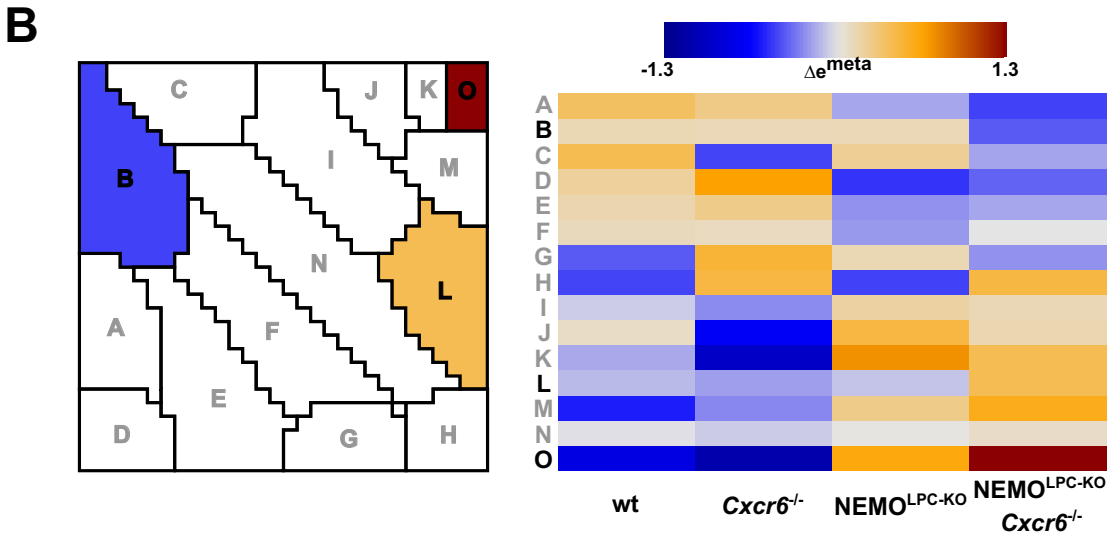


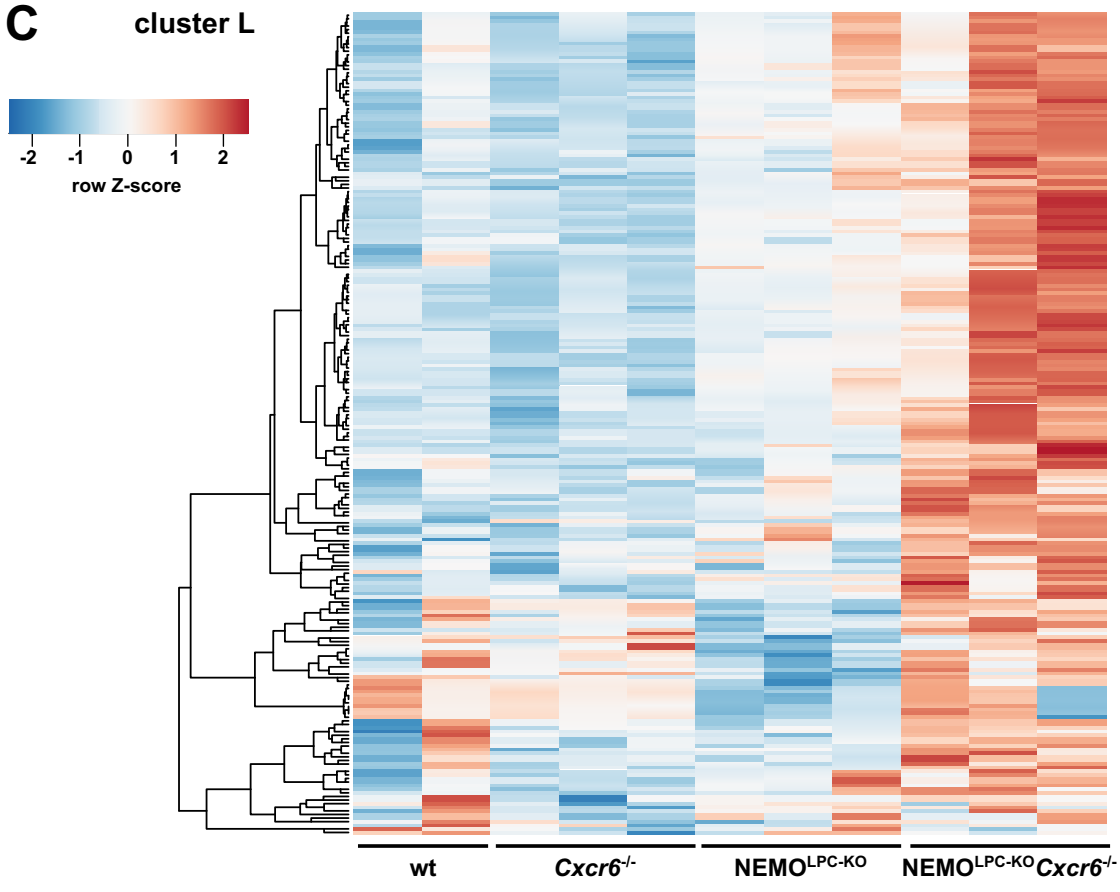


(caption on next page)

**Fig. 4.** Self-organizing maps reveal sample-specific co-expression clusters. Purified RNA from isolated hepatocytes from wt (n = 2), *Cxcr6*$^{-/-}$ (n = 3), NEMO$^{LPC\text{-}KO}$ (n = 3) and NEMO$^{LPC\text{-}KO}$*Cxcr6*$^{-/-}$ (n = 3) mice were subjected to microarray analysis. Co-regulated transcripts were identified by an analysis and visualization method based on self-organizing maps (SOM) machine learning. (A) SOM portraits using a 30 × 30 mosaic grid. The color gradient visualizes over- and under-expression of the metagenes compared with the mean expression level in the pool of all samples, indicating regions of over- and underexpression by red and blue spots, respectively. (B) Overexpression spots representing clusters of co-expressed metagenes identified by K-means hierarchical clustering (left panel). Overexpression summary heatmap of 15 identified clusters. The expression scale refers to the metagene of maximum expression in the respective cluster. (C) Clustered Heatmap of the standardized mRNA expression of genes belonging to cluster L with high expression in NEMO$^{LPC\text{-}KO}$*Cxcr6*$^{-/-}$ mice.

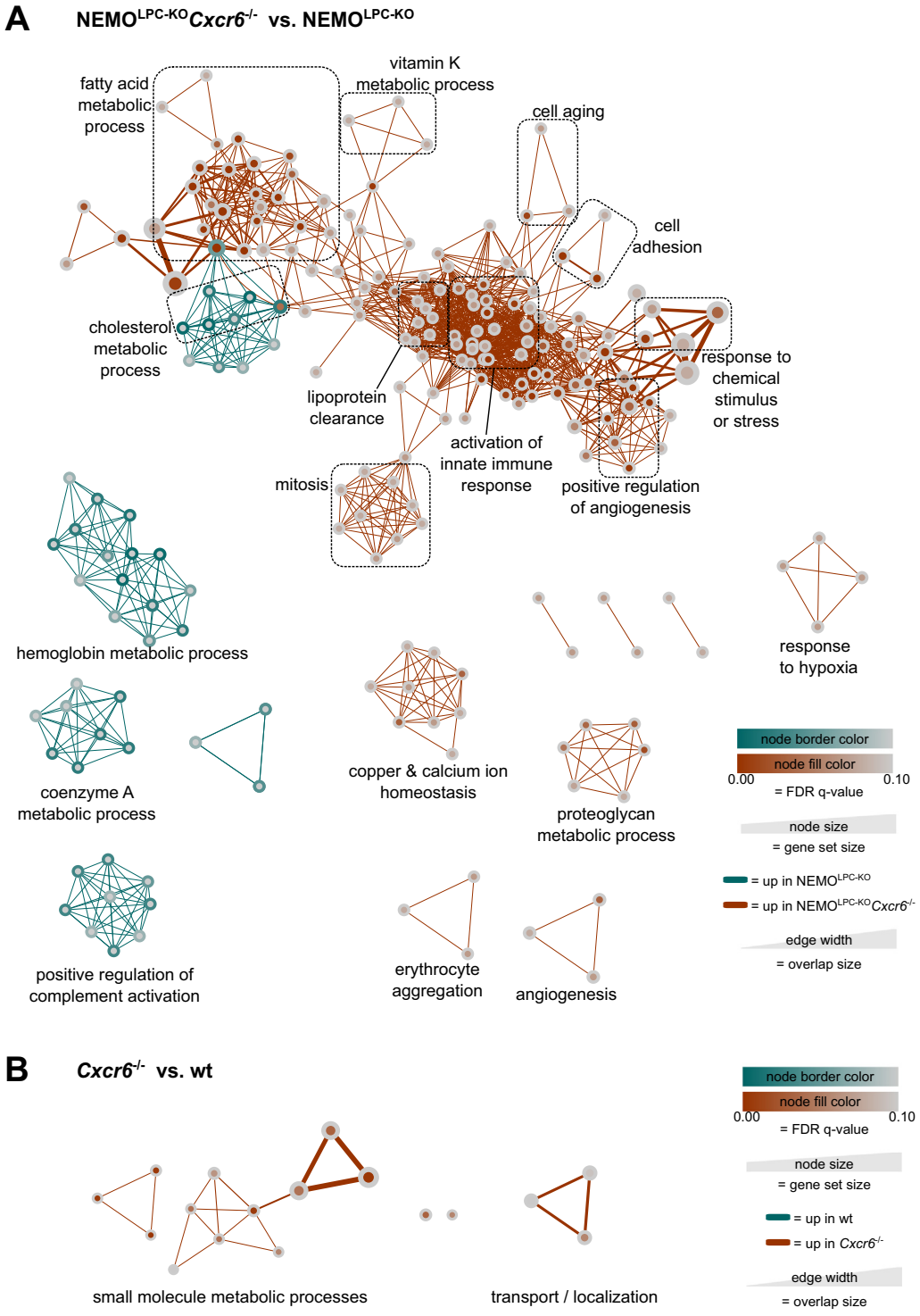


**Fig. 5.** Pathway regulation in hepatocytes from NEMO$^{LPC\text{-}KO}$ and NEMO$^{LPC\text{-}KO}$*Cxcr6*$^{-/-}$ mice. Differentially regulated genes were selected by the ANOVA p-value ($p \leq 0.05$) and their fold change ($\geq 2$ or $\leq -2$). Enriched GO biological process terms were identified and visualized as clustered enrichment map of significantly regulated ($p \leq 0.01$) terms comparing NEMO$^{LPC\text{-}KO}$*Cxcr6*$^{-/-}$ with NEMO$^{LPC\text{-}KO}$ (A) and *Cxcr6*$^{-/-}$ with wt (B). Please note the much more complex pathway regulation on the NEMO$^{LPC\text{-}KO}$ (A) vs the wt (B) background.

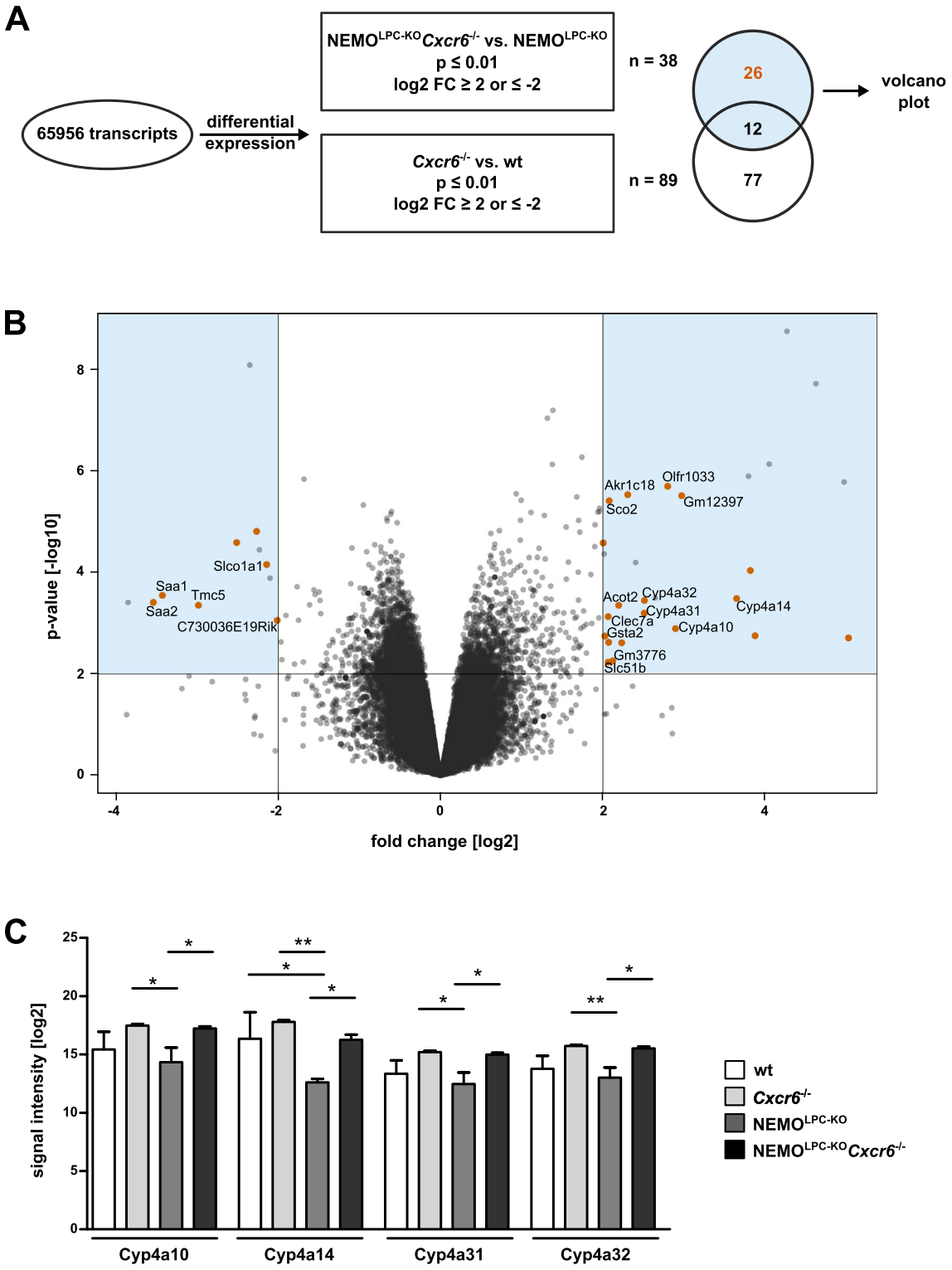


**Fig. 6.** Members of the cytochrome P450 4a family are specifically upregulated in hepatocytes from NEMO$^{LPC\text{-}KO}$*Cxcr6*$^{-/-}$ vs. NEMO$^{LPC\text{-}KO}$ mice. (A) Schematic overview of the gene selection for the volcano plot displayed in Fig. 6B. (B) Volcano plot showing log2 fold change and p-value of each transcript comparing NEMO$^{LPC\text{-}KO}$*Cxcr6*$^{-/-}$ with NEMO$^{LPC\text{-}KO}$. Blue boxes indicate significantly regulated genes by a threshold of $p \leq 0.01$ and log2 FC $\geq 2$ or $\leq -2$. Orange colored dots mark transcripts, which do not pass the threshold when comparing *Cxcr6*$^{-/-}$ with wt. If applicable, gene symbols are plotted. (C) Log2 signal intensity from the microarrays of the four cytochrome P450 family 4a members. All data are represented as mean ± SD. *$p < 0.05$, **$p < 0.01$ (one-way ANOVA).

by orange color. This analysis revealed that four members of the cytochrome P450 family 4a (Cyp4a10, Cyp4a14, Cyp4a31, Cyp4a32) were specifically regulated in the NEMO$^{LPC\text{-}KO}$*Cxcr6*$^{-/-}$ vs. NEMO$^{LPC\text{-}KO}$ comparison (see also Suppl. Table S3). By contrast, Cyp2e1 - the most abundant cytochrome P450 in hepatocytes - was not regulated in any of the samples. Regarding the signal intensity on the microarrays, expression of the four Cyp4a family members was elevated in both genotypes, where CXCR6 is deleted, and further displayed a trend

towards downregulation in the NEMO$^{LPC-KO}$ (Fig. 6C). in summary, a number of pathways related to stress response and metabolism were significantly regulated in hepatocytes dependent on CXCR6-deficiency, with Cyp4a being an example for an activated gene family in CXCR6-deficient hepatocytes.

### 3.5. CXCR6 protects from TNF-α-induced hepatotoxicity

Based on our findings from the microarray analysis, we hypothesized that NEMO-deficient hepatocytes, which developed in a CXCR6-deficient environment, were particularly susceptible to stress signals.

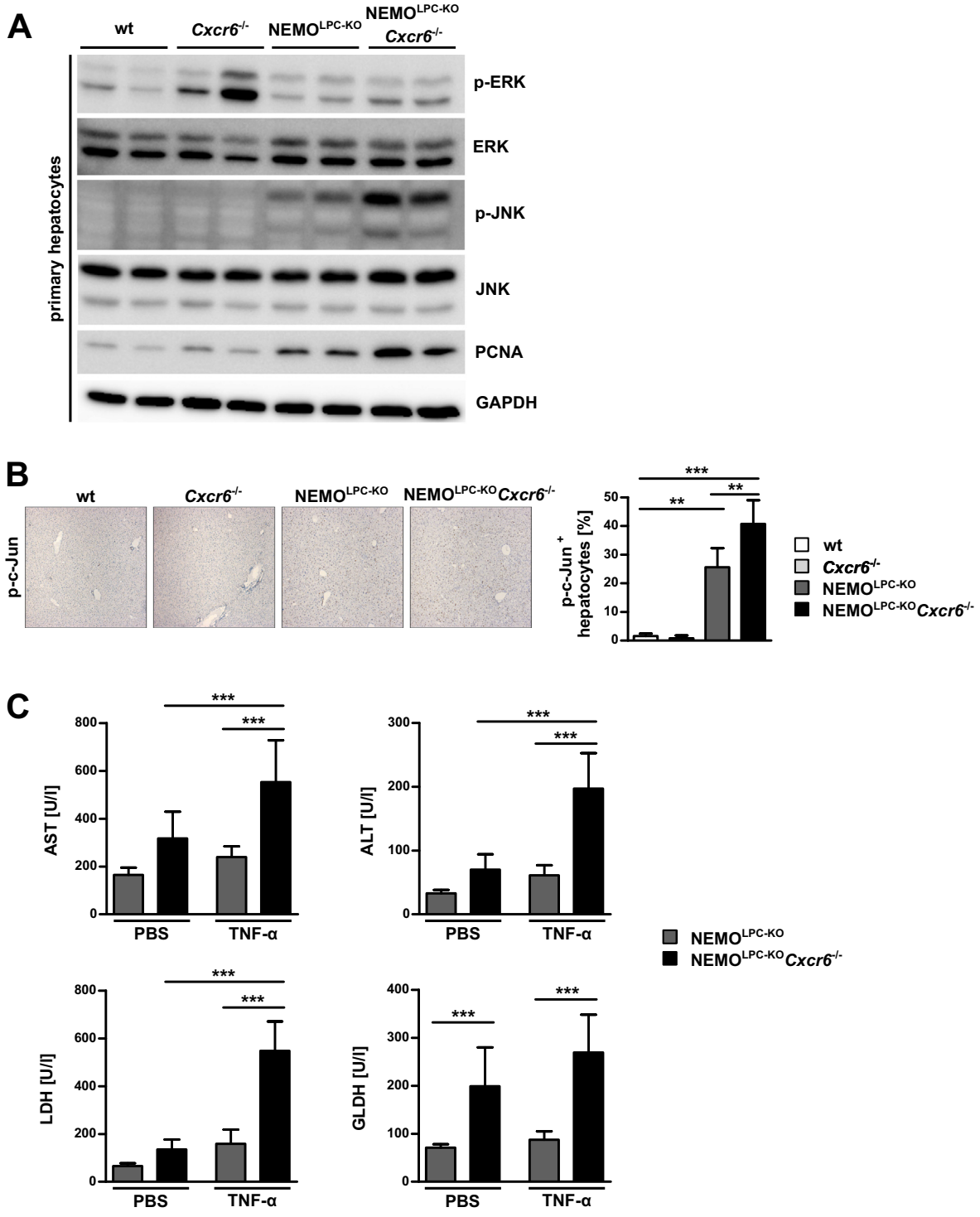


**Fig. 7.** Primary hepatocytes from NEMO$^{LPC-KO}$*Cxcr6*$^{-/-}$ mice are more susceptible to TNF-α induced injury then hepatocytes from NEMO$^{LPC-KO}$ mice. (A) Protein expression and phosphorylation of the MAP kinases ERK and JNK and protein expression of proliferating cell nuclear antigen (PCNA) was analyzed by western blotting in protein lysates from hepatocytes isolated from 8 week old mice. Biological replicates of n = 2 animals per genotype. (B) Immunohistochemical staining for phosphorylated c-Jun (p-c-Jun) in liver sections of 8 week old mice, representative images (left panel), quantification of p-c-Jun$^{+}$ hepatocytes (right panel). Biological replicates of n = 3 to 6 animals per genotype. (C) Freshly isolated hepatocytes from 12 week old mice were plated on tissue culture plates and treated with 100 ng TNF-α for 10 h. Hepatocyte injury was assessed by transaminase, LDH and GLDH activities in the culture supernatant. Biological replicates of n = 2 to 3 per data point and technical replicates of n = 2 to 5 per biological replicate. All data are represented as mean ± SD. **p < 0.01, ***p < 0.001 (one-way ANOVA).

Thus, we investigated activation of kinases from MAPK signaling pathways in isolated hepatocytes. Phosphorylation of ERK1 and ERK2 was strongly induced in hepatocytes from *Cxcr6*$^{-/-}$ mice in comparison to their wt or NEMO$^{LPC-KO}$ counterparts (Fig. 7A). Moreover, phosphorylation of the c-Jun N-terminal kinases (JNK) was primarily detectable in NEMO$^{LPC-KO}$*Cxcr6*$^{-/-}$ hepatocytes. JNK is a mediator of TNF-α- or oxidative stress-induced cell death in the liver but is also important for compensatory proliferation and regeneration in response to apoptosis [24,25]. Expression of the cell cycle activation marker Proliferating-Cell-Nuclear-Antigen (PCNA) was strongly enhanced in hepatocytes from NEMO$^{LPC-KO}$*Cxcr6*$^{-/-}$ mice (Fig. 7A). Furthermore, staining for phosphorylated c-Jun in liver sections was augmented in NEMO$^{LPC-KO}$ and NEMO$^{LPC-KO}$*Cxcr6*$^{-/-}$ mice, with a significantly higher number of phosho-c-Jun$^{+}$ hepatocytes in the latter (Fig. 7B). The transcription factor c-Jun is a downstream phosphorylation target of JNK and associated with proliferation. Finally, to test how hepatocyte death is affected by the loss of CXCR6 in NEMO$^{LPC-KO}$ mice, primary cultured hepatocytes were treated with TNF-α and hepatocyte death was monitored by serum transaminase as well as lactate and glutamate dehydrogenase (LDH, GLDH) activities in the cell culture supernatant. NEMO$^{LPC-KO}$*Cxcr6*$^{-/-}$ hepatocytes already displayed a basal activation when treated with PBS alone, which was even enhanced when TNF-α was added to the cells (Fig. 7C). These results demonstrated that in hepatocytes from NEMO$^{LPC-KO}$*Cxcr6*$^{-/-}$ pathways of stress responses, inflammation and compensatory proliferation are more activated and these cells are more susceptible to TNF-α- induced hepatotoxicity.

## 4. Discussion

The genetic deletion of the NF-κB regulatory subunit NEMO in liver parenchymal cells is an established mouse model to study mechanisms of hepatic injury, inflammation and fibrosis [1]. In the present study, we could show that the additional deletion of the chemokine receptor CXCR6 in the NEMO$^{LPC-KO}$ background not only aggravates early inflammation and fibrosis, but sensitizes hepatocytes to TNF-α induced cell death. NEMO$^{LPC-KO}$*Cxcr6*$^{-/-}$ mice showed signs of enhanced liver damage and fibrosis, a higher number of macrophages, pro-inflammatory cytokine expression and apoptosis compared to NEMO$^{LPC-KO}$ mice. This is a surprising result, since deletion of CXCR6 had a protective effect in models of acute and chronic liver inflammation [5,12]. Interestingly, adoptive transfer of CXCR6$^{+}$ cells was not able to protect NEMO$^{LPC-KO}$*Cxcr6*$^{-/-}$ mice from increased hepatocyte damage. This implies that neither CXCR6$^{+}$ (immune) cells nor CXCR6-dependent signaling could be beneficial for these mice and that presumably the hepatocytes themselves seem to be the underlying cause for the inflammatory, fibrotic phenotype. This hypothesis is further strengthened by the observation that transfer of CXCR6$^{+}$ cells to NEMO$^{LPC-KO}$ mice, but not to NEMO$^{LPC-KO}$*Cxcr6*$^{-/-}$ mice, was able to restore the hepatic injury to nearly wt conditions. Hence, providing CXCR6$^{+}$ cells to mice with intact CXCR6 signaling and cell populations is beneficial in the context of LPC-specific deletion of NEMO, but not when CXCR6 is deleted as well.

Microarray analysis of isolated hepatocytes revealed that although hepatocytes do not express CXCR6 (data not shown) they displayed striking differences in their transcriptome dependent on the CXCR6-proficient or -deficient background. Pathways related to innate immune response, stress response and fatty acid metabolism were upregulated in hepatocytes from NEMO$^{LPC-KO}$*Cxcr6*$^{-/-}$ mice compared to NEMO$^{LPC-KO}$ mice. Additionally, MAPK signaling was identified as an over-represented pathway in a cluster of co-regulated genes specifically overexpressed in NEMO$^{LPC-KO}$*Cxcr6*$^{-/-}$ mice. This implicates that hepatocytes from NEMO$^{LPC-KO}$*Cxcr6*$^{-/-}$ mice seem to be particularly “on alert”. It is known that, because of interrupted NF-κB signaling, hepatocytes from NEMO$^{LPC-KO}$ mice are hyperreactive to TNF-α [1]. When CXCR6 is additionally deleted, hepatocytes were even more prone to TNF-α-induced cell death. Furthermore, several marker proteins for compensatory proliferation were induced in hepatocytes from NEMO$^{LPC-KO}$*Cxcr6*$^{-/-}$ mice.

It has been suggested that the CXCR6/CXCL16 axis promotes liver diseases, such as acute liver injury [12,26], fibrosis [5], or NAFLD [9–11], based on experimental data and correlations observed in patients. In the setting of hepatic inflammation and fibrosis driven by the LPC-specific knockout of NEMO, however, the loss of CXCR6 is detrimental. In this regard, this genetic model is quite unique, because the onset of the disease takes place very early, as already 3 week old mice show increased liver damage [1]. Unfortunately, no “floxed” CXCR6 mice are available that would allow a cell-type specific or a inducible CXCR6 depletion. It would indeed be interesting to investigate, whether a transient deletion of Cxcr6 showed similar results.

Several studies could convincingly demonstrate that liver sinusoidal endothelial cells (LSECs) are the predominant source of CXCL16 in the liver [6,27]. Moreover, some reports indicated CXCL16 expression also in hepatocytes, although at moderate levels [11,28]. In our hepatocyte microarray data, CXCL16 signal intensity was below that of internal negative controls. Moreover, neutralization of CXCL16 by an antibody for 4 weeks did not ameliorate liver injury in 8 weeks old NEMO$^{LPC-KO}$*Cxcr6*$^{-/-}$ mice (detailed data not shown). Therefore, a CXCL16-mediated signaling in the hepatocytes is unlikely the cause of liver damage.

Taking together, these results suggested that the hepatocytes from double knockout mice are more vulnerable due to the loss of CXCR6, although they are not involved in the CXCR6-CXCL16 axis themselves. Increased hepatocyte death may lead to enhanced inflammatory responses, compensatory proliferation and as a result to increased fibrosis already at a very early age. Since adoptive transfer of CXCR6-expressing cells beginning at 4 weeks of age did not alter hepatocyte damage, “priming” must take place earlier in development, and further studies will be needed to address these mechanisms.

Another interesting finding from the transcriptome analysis was that four members of the cytochrome P450 family 4a were specifically upregulated in NEMO$^{LPC-KO}$*Cxcr6*$^{-/-}$ mice. This family comprises at least 9 isoforms in mice: Cyp4a-10, −12a, −12b, −14, −28-ps, −29, −30b, −31 and −32, with Cyp4a-28-ps being a non-protein-coding pseudogene. Cyp4a enzymes are fatty acid hydroxylases and involved in microsomial ω-oxidation of free fatty acids in the liver [29]. In our analysis Cyp4a10, −14, −31 and −32 were specifically upregulated in in NEMO$^{LPC-KO}$*Cxcr6*$^{-/-}$ mice compared to in NEMO$^{LPC-KO}$ mice, but displayed also high mRNA expression in *Cxcr6*$^{-/-}$ mice. It has been shown that Cyp4a10 and −14 are also upregulated in the livers of diabetic mice and that inhibition of Cyp4A reduces hepatic ER stress, apoptosis, insulin resistance and steatosis [30]. Hepatic Cyp4a14 expression has been found to be upregulated in three different mouse models of non-alcoholic fatty liver disease (NAFLD), and expression of the main Cyp4a enzyme in humans, Cyp4a11, in NAFLD patients is increased as well [31]. The same study could demonstrate that in the absence of Cyp4a14 MCD diet-fed mice display reduced hepatic lipid accumulation, inflammation and fibrosis [31], which fits well to the Cyp4a induction observed in hepatocytes of NEMO$^{LPC-KO}$*Cxcr6*$^{-/-}$ mice. These observations may suggest interactions between immune mechanisms and hepatocyte metabolism involving Cyp4a as a risk factor for liver injury and steatohepatitis.

## 5. Conclusions

Altogether, our study emphasizes the ambiguity of inflammatory responses in the complex interplay of parenchymal cells and infiltrating immune cells in the liver. While CXCR6-mediated immune cell recruitment aggravates classical models of acute or chronic liver injury in mice, their genetic depletion enhances cell death, inflammation and proliferation of hepatocytes in the NEMO$^{LPC-KO}$ background. These data demonstrate a novel role of CXCR6 for stress responses in hepatocytes,

independent from the functions of CXCR6 on immune cells.

Supplementary data to this article can be found online at https://doi.org/10.1016/j.bbadis.2018.11.020.

## Author contributions

F.T. designed and guided the research. A.W., J.C.M. and M.K. performed the animal experiments. A.W. performed hepatocyte cultures and hydroxyproline assays. J.C.M. performed the qPCR analysis. K.K. performed histological stainings and immunoblot analyses. A.L. and A.W. analyzed the data. B.D. performed microarray analysis and data processing. A.L. and I.G.C. performed bioinformatic data analysis of microarray data. C.T. and T.L. contributed to research design and provided important technical support and intellectual input. A.L. and F.T. wrote the manuscript. All authors reviewed and approved the manuscript.

## Transparency document

The Transparency document associated with this article can be found, in online version.

## Acknowledgements

This work was supported by the German Research Foundation (DFG; Ta434/3-1 and SFB/TRR57) and the Interdisciplinary Center for Clinical Research (IZKF) Aachen.

## Conflict of interest

The authors disclose no conflict of interest related to this work.

## References

[1] T. Luedde, et al., Deletion of NEMO/IKKgamma in liver parenchymal cells causes steatohepatitis and hepatocellular carcinoma, Cancer Cell 11 (2007) 119–132, https://doi.org/10.1016/j.ccr.2006.12.016.
[2] M. Ringelhan, D. Pfister, T. O'Connor, E. Pikarsky, M. Heikenwalder, The immunology of hepatocellular carcinoma, Nat. Immunol. 19 (2018) 222–232, https://doi.org/10.1038/s41590-018-0044-z.
[3] K. Bettermann, et al., TAK1 suppresses a NEMO-dependent but NF-kappaB-independent pathway to liver cancer, Cancer Cell 17 (2010) 481–496, https://doi.org/10.1016/j.ccr.2010.03.021.
[4] T. Luedde, N. Kaplowitz, R.F. Schwabe, Cell death and cell death responses in liver disease: mechanisms and clinical relevance, Gastroenterology 147 (2014) 765–783 e764 https://doi.org/10.1053/j.gastro.2014.07.018.
[5] A. Wehr, et al., Chemokine receptor CXCR6-dependent hepatic NK T cell accumulation promotes inflammation and liver fibrosis, J. Immunol. 190 (2013) 5226–5236, https://doi.org/10.4049/jimmunol.1202909.
[6] F. Geissmann, et al., Intravascular immune surveillance by CXCR6+ NKT cells patrolling liver sinusoids, PLoS Biol. 3 (2005) e113, , https://doi.org/10.1371/journal.pbio.0030113.
[7] A. Wehr, F. Tacke, The roles of CXCL16 and CXCR6 in liver inflammation and fibrosis, Curr. Pathobiol. Rep. 3 (2015) 283–290, https://doi.org/10.1007/s40139-015-0090-2.
[8] F. Heymann, et al., Long term intravital multiphoton microscopy imaging of immune cells in healthy and diseased liver using CXCR6.Gfp reporter mice, J. Vis. Exp. (2015), https://doi.org/10.3791/52607.
[9] K.L. Ma, et al., Activation of the CXCL16/CXCR6 pathway promotes lipid deposition in fatty livers of apolipoprotein E knockout mice and HepG2 cells, Am. J. Transl. Res. 10 (2018) 1802–1816.
[10] S. Zhang, et al., Hepatic CXCL16 is increased in gallstone accompanied with liver injury, Eur. J. Clin. Investig. 47 (2017) 667–674, https://doi.org/10.1111/eci.12788.
[11] L. Jiang, et al., CXC motif ligand 16 promotes nonalcoholic fatty liver disease progression via hepatocyte-stellate cell crosstalk, J. Clin. Endocrinol. Metab. 103 (2018) 3974–3985, https://doi.org/10.1210/jc.2018-00762.
[12] A. Wehr, et al., Pharmacological inhibition of the chemokine CXCL16 diminishes liver macrophage infiltration and steatohepatitis in chronic hepatic injury, PLoS One 9 (2014) e112327, , https://doi.org/10.1371/journal.pone.0112327.
[13] D. Unutmaz, et al., The primate lentiviral receptor Bonzo/STRL33 is coordinately regulated with CCR5 and its expression pattern is conserved between human and mouse, J. Immunol. 165 (2000) 3284–3292.
[14] K.R. Karlmark, et al., Hepatic recruitment of the inflammatory Gr1+ monocyte subset upon liver injury promotes hepatic fibrosis, Hepatology 50 (2009) 261–274, https://doi.org/10.1002/hep.22950.
[15] A.T. Schneider, et al., RIPK1 suppresses a TRAF2-dependent pathway to liver cancer, Cancer Cell 31 (2017) 94–109, https://doi.org/10.1016/j.ccell.2016.11.009.
[16] F. Heymann, et al., Hepatic macrophage migration and differentiation critical for liver fibrosis is mediated by the chemokine receptor C-C motif chemokine receptor 8 in mice, Hepatology 55 (2012) 898–909, https://doi.org/10.1002/hep.24764.
[17] R.A. Irizarry, et al., Exploration, normalization, and summaries of high density oligonucleotide array probe level data, Biostatistics 4 (2003) 249–264, https://doi.org/10.1093/biostatistics/4.2.249.
[18] H. Loffler-Wirth, M. Kalcher, H. Binder, oposSOM: R-package for high-dimensional portraying of genome-wide expression landscapes on bioconductor, Bioinformatics 31 (2015) 3225–3227, https://doi.org/10.1093/bioinformatics/btv342.
[19] H. Wirth, M. Loffler, M. von Bergen, H. Binder, Expression cartography of human tissues using self organizing maps, BMC Bioinf. 12 (2011) 306, https://doi.org/10.1186/1471-2105-12-306.
[20] H. Mi, et al., PANTHER version 11: expanded annotation data from Gene Ontology and Reactome pathways, and data analysis tool enhancements, Nucleic Acids Res. 45 (2017) D183–D189, https://doi.org/10.1093/nar/gkw1138.
[21] P. Shannon, et al., Cytoscape: a software environment for integrated models of biomolecular interaction networks, Genome Res. 13 (2003) 2498–2504, https://doi.org/10.1101/gr.1239303.
[22] S. Maere, K. Heymans, M. Kuiper, BiNGO: a cytoscape plugin to assess overrepresentation of gene ontology categories in biological networks, Bioinformatics 21 (2005) 3448–3449, https://doi.org/10.1093/bioinformatics/bti551.
[23] D. Merico, R. Isserlin, O. Stueker, A. Emili, G.D. Bader, Enrichment map: a network-based method for gene-set enrichment visualization and interpretation, PLoS One 5 (2010) e13984, , https://doi.org/10.1371/journal.pone.0013984.
[24] M. Vucur, et al., RIP3 inhibits inflammatory hepatocarcinogenesis but promotes cholestasis by controlling caspase-8- and JNK-dependent compensatory cell proliferation, Cell Rep. 4 (2013) 776–790, https://doi.org/10.1016/j.celrep.2013.07.035.
[25] R.F. Schwabe, et al., c-Jun-N-terminal kinase drives cyclin D1 expression and proliferation during liver regeneration, Hepatology 37 (2003) 824–832, https://doi.org/10.1053/jhep.2003.50135.
[26] H. Wang, et al., CXCL16 deficiency attenuates acetaminophen-induced hepatotoxicity through decreasing hepatic oxidative stress and inflammation in mice, Acta Biochim. Biophys. Sin. 49 (2017) 541–549, https://doi.org/10.1093/abbs/gmx040.
[27] C. Ma, et al., Gut microbiome-mediated bile acid metabolism regulates liver cancer via NKT cells, Science 360 (2018), https://doi.org/10.1126/science.aan5931.
[28] M. Heydtmann, et al., CXC chemokine ligand 16 promotes integrin-mediated adhesion of liver-infiltrating lymphocytes to cholangiocytes and hepatocytes within the inflamed human liver, J. Immunol. 174 (2005) 1055–1062.
[29] R. Gambino, G. Musso, M. Cassader, Redox balance in the pathogenesis of non-alcoholic fatty liver disease: mechanisms and therapeutic opportunities, Antioxid. Redox Signal. 15 (2011) 1325–1365, https://doi.org/10.1089/ars.2009.3058.
[30] E.C. Park, et al., Inhibition of CYP4A reduces hepatic endoplasmic reticulum stress and features of diabetes in mice, Gastroenterology 147 (2014) 860–869, https://doi.org/10.1053/j.gastro.2014.06.039.
[31] X. Zhang, et al., Ablation of cytochrome P450 omega-hydroxylase 4A14 gene attenuates hepatic steatosis and fibrosis, Proc. Natl. Acad. Sci. U. S. A. 114 (2017) 3181–3185, https://doi.org/10.1073/pnas.1700172114.